

Derivation of Forcing Functions for Monte Carlo Atmospheric Gust Loads Analysis

July 1999

Prepared by

B. H. SAKO, M. C. KIM, A. M. KABE, W. K. YEUNG
Structural Dynamics Department

Prepared for

SPACE AND MISSILE SYSTEMS CENTER
AIR FORCE MATERIEL COMMAND
2430 E. El Segundo Boulevard
Los Angeles Air Force Base, CA 90245

Contract No. F04701-93-C-0094

Engineering and Technology Group

This report was submitted by The Aerospace Corporation, El Segundo, CA 90245-4691, under Contract No. F04701-93-C-0094 with the Space and Missile Systems Center, P. O. Box 92960, Los Angeles, CA 90009-2960. It was reviewed and approved for The Aerospace Corporation by R. W. Fillers, Principal Director. The project officer is Maj. Charles R. Williamson.

This report has been reviewed by the Public Affairs Office (PAS) and is releasable to the National Technical Information Service (NTIS). At NTIS, it will be available to the general public, including foreign nationals.

This technical report has been reviewed and is approved for publication. Publication of this report does not constitute Air Force approval of the report's findings or conclusions. It is published only for the exchange and stimulation of ideas.

A handwritten signature in cursive script, reading "Charles R. Williamson". The signature is written in dark ink and is positioned above the printed name and title.

Maj. Charles R. Williamson
Project Officer

REPORT DOCUMENTATION PAGEForm Approved
OMB No. 0704-0188

Public reporting burden for this collection of information is estimated to average 1 hour per response, including the time for reviewing instructions, searching existing data sources, gathering and maintaining the data needed, and completing and reviewing the collection of information. Send comments regarding this burden estimate or any other aspect of this collection of information, including suggestions for reducing this burden, to Washington Headquarters Services, Directorate for Information Operations and Reports, 1215 Jefferson Davis Highway, Suite 1204, Arlington, VA 22202-4302, and to the Office of Management and Budget, Paperwork Reduction Project (0704-0188), Washington, DC 20503.

1. AGENCY USE ONLY (Leave blank)

2. REPORT DATE

3. REPORT TYPE AND DATES COVERED

July 1999

Final

4. TITLE AND SUBTITLE

Derivation of Forcing Functions for Monte Carlo Atmospheric Gust Loads Analysis

5. FUNDING NUMBERS

F04701-93-C-0094

6. AUTHOR(S)

B. H. Sako, M. C. Kim, A. M. Kabe, W. K. Yeung

7. PERFORMING ORGANIZATION NAME(S) AND ADDRESS(ES)

The Aerospace Corporation
2350 E. El Segundo Boulevard
El Segundo, CA 902458. PERFORMING ORGANIZATION
REPORT NUMBER

TR-99(1534)-6

9. SPONSORING/MONITORING AGENCY NAME(S) AND ADDRESS(ES)

Space and Missile Systems Center
Air Force Materiel Command
2430 E. El Segundo Boulevard
Los Angeles Air Force Base, CA 9024510. SPONSORING/MONITORING
AGENCY REPORT NUMBER

SMC-TR-00-25

11. SUPPLEMENTARY NOTES

12a. DISTRIBUTION/AVAILABILITY STATEMENT

Approved for public release; distribution unlimited

12b. DISTRIBUTION CODE

13. ABSTRACT (Maximum 200 words)

A methodology developed to derive forcing functions from the turbulent component of measured wind profiles for a new Monte Carlo gust loads analysis approach is described. Several large sets of forcing functions were developed by extracting the short-duration, random component of measured Jimsphere wind profiles. A database consisting of Jimsphere wind soundings measured over the past three decades at the Eastern and Western Ranges of the United States was used to derive the forcing functions. Validity of these forcing functions for heavy-lift and medium-lift launch vehicles was established by examining the error contributions from various sources within the wind measurement system and the application of a noise-reducing filter. A unique aspect of the method is the extraction of the relatively rapidly changing turbulent component associated with the non-persistent wind features which are expected over a given observation time period.

14. SUBJECT TERMS

Gust forcing functions, Jimsphere, wind profiles, atmospheric flight loads, launch vehicles

15. NUMBER OF PAGES

45

16. PRICE CODE

17. SECURITY CLASSIFICATION
OF REPORT

Unclassified

18. SECURITY CLASSIFICATION
OF THIS PAGE

Unclassified

19. SECURITY CLASSIFICATION
OF ABSTRACT

Unclassified

20. LIMITATION OF ABSTRACT

Abstract

A methodology is developed to derive gust forcing functions from the turbulent components of measured wind profiles. Several large sets of forcing functions were developed by extracting the short-duration, random component of measured Jimsphere wind profiles. A database consisting of Jimsphere wind soundings measured over the past three decades at the Eastern and Western Ranges of the United States was used to derive the forcing functions. Validity of these forcing functions for heavy-lift and medium-lift launch vehicles was established by examining the error contributions from various sources within the wind measurement system and the application of a noise reducing filter. A unique aspect of the method is the extraction of the relatively rapidly changing turbulent component associated with the non-persistent wind features which are expected over a given observation time period. The gust forcing functions can be used in a Monte Carlo analysis to determine launch vehicle loads for the Eastern and Western Ranges.

Contents

Abstract.....	1
Acknowledgments.....	5
Nomenclature	7
1. Introduction.....	9
2. Jimsphere-Rose System.....	11
3. Accuracy of Wind Profiles	13
3.1. Amplitude and Phase Response.....	13
3.2. Rose Processing Effects.....	16
3.3. Self-Induced Oscillations and Aliasing Errors.....	19
3.4. Radar Errors	21
4. Validity of Wind-Derived Forcing Functions.....	23
5. Wind Database Description.....	25
6. Forcing Functions Derivation.....	27
6.1. Removal of Noise Floor.....	27
6.2. Extraction of Turbulent Wind Features.....	31
6.3. Restriction to 6000-ft Bands.....	34
6.4. Screening of Wind Data Using a Shear Criterion.....	34
7. Results	37
7.1 A Practical Consideration.....	39
8. Conclusions.....	41
References	43

Figures

1,	Amplification factor and phase response plots for Jimsphere at 30 kft and 45 kft	15
2a.	AF_{Rose} at various averaging layer lengths.....	18
2b.	Verifying AF_{Rose} by comparing to attenuation factors from Rose program simulation using sinusoidal wind fields at various wavelengths.....	18
3.	Combined amplification factor from Jimsphere and Rose program is less than 5% to >500 ft	19
4.	Power Spectral Density of U and V wind components of a typical Jimsphere wind profile shows the self induced oscillation and the noise floor	20
5.	Nyquist folding diagram showing how self-induced oscillations at 72–82 ft are aliased to wavelengths at 450–250 ft due to the Rose program's 100-ft sampling	21
6.	Monthly distributions of WR (a) and ER (b) Jimsphere wind profiles.....	25
7.	Yearly distributions of Jimsphere wind profiles for WR (a) and ER (b)	25
8.	Two examples of method used to drive forcing functions	27
9.	Ensemble averages of wind magnitude PSDs from WR and ER obeying the power law with $\lambda \approx 2.7$	29
10.	a) Comparison of unfiltered and 2-point filtered wind profile; b) Noise removed by the filtering process.....	30
11.	Two-point filtering removes noise floor having a flat spectrum and extends the usable spectrum to include wavelengths ≥ 500 ft.....	31
12.	Ensemble averages of filtered wind PSDs for $\lambda_G = 3300, 4200$, and 4700 ft.....	32
13.	a) Two-point smoothed wind and trend removed for $\lambda_G = 3300$ ft; b) High-passed filtered wind profile	33
14.	a) Two-point smoothed wind and trend removed for $\lambda_G = 4200$ ft; b) High-passed filtered wind profile	33
15.	a) Two-point smoothed wind and trend removed for $\lambda_G = 4700$ ft; b) High-passed filtered wind profile	34
16.	Wind profile with $dW / dh _{\text{max}} \approx 0.28 \text{ sec}^{-1}$ and failing the shear criteria. ($\lambda_G = 3300$ ft)	35
17.	Forcing function comparisons using different λ_G	37
18.	Forcing function comparisons using different λ_G	38
19.	Forcing function comparisons using different λ_G	39

Acknowledgments

The authors are grateful to Dr. Richard L. Walterscheid for his helpful comments and suggestions and to Timothy L. Wilfong for providing a version of the Rose program.

Nomenclature

A	wind velocity amplitude, ft/s
AF_B	balloon's response amplification factor
AF_{Rose}	Rose program amplification factor
D_B	balloon's diameter, ft
f	wavenumber, cycles/ft
g	gravitational acceleration, ft/s ²
G	wind speed power spectral density, ft ³ /s ² /cycle
h	altitude, ft
H_{opt}	optimal filter's frequency response
L_{avg}	Rose program averaging layer length, ft
L	balloon's lag distance, ft
m_A	balloon's apparent mass, lb
m_B	balloon's mass, lb
m_0	balloon's displaced mass, lb
n	wind measurement noise, ft/s
R	balloon's response distance, ft
Re	Reynolds number
U	wind velocity in the east-west direction, ft/s
V	wind velocity in the north-south direction, ft/s
W	one-dimensional wind field, ft/s
W_X	wind field in the x direction, ft/s
\hat{W}	measured one-dimensional wind field, ft/s
\dot{x}_B	balloon's horizontal velocity, ft/s
\dot{z}_B	balloon's rise rate, ft/s
γ	wind's spectral density power law exponent
λ	vertical wavelength of horizontal wind field, ft
λ_B	wavelength defining the boundary between persistent and non-persistent wind features, ft
λ_G	high-pass filter's corner wavelength used to extract turbulent wind features, ft
ν	kinematic viscosity of air, ft ² /s
ρ_A	ambient density of atmosphere, lb/ft ³
ϕ_B	balloon's phase response, rad
ω	atmospheric bouyancy frequency, cycles/s

1. Introduction

Gust loads analyses are performed to establish structural loads that a launch vehicle and its payload may experience as a result of atmospheric turbulence. Because these loads are driven by relatively rapidly changing wind features, gust loads must be determined statistically.

Current analysis procedures employ synthetic gust velocity profiles that are designed to yield loads of a desired level of statistical conservatism.¹ Typically, the analysis is performed by instantaneously enveloping the launch vehicle in the selected gust velocity profile. Parameters such as amplitude, shape, and wavelength of the synthetic gusts are selected to induce in the launch vehicle/payload system a desired level of load. The most common waveform currently used is a one-minus cosine shape; on some vehicles a one-minus cosine with a flattop is used (Ref. 1). Other profiles have also been proposed.²

Work to date has concentrated on analysis of wind features to establish the shape and magnitude of the synthetic profiles, or to develop a statistical description of atmospheric turbulence.³⁻¹⁴ However, none of these efforts has established the loads of launch vehicles subjected to actual short duration atmospheric turbulence. This paper will present a methodology that extracts the turbulent component from measured wind profiles to define empirical forcing functions that can be used in Monte Carlo gust loads analyses.¹⁵ Several large sets of forcing functions were developed by extracting the short-duration, random component of measured Jimsphere wind profiles. A database consisting of over 1000 Western Range (WR) and over 1000 Eastern Range (ER) wind soundings, dating from 1964 to 1997, was used to derive the forcing functions.

2. Jimsphere-Rose System

Over the last several decades, horizontal wind fields as a function of altitude have been measured in the United States at both the Eastern Range (ER) in Florida and the Western Range (WR) in California using radar-tracked Jimsphere balloons.

The Jimsphere is a 6.5 ft diameter, rigid spherical balloon constructed of 0.5 mil aluminized Mylar.¹⁶ Rigidity is accomplished by maintaining an internal overpressure using valves 180 deg apart which vent helium as the balloon rises. The balloon's surface is roughened by 398 conical elements to reduce both amplitude and spectral bandwidth of the lateral self-induced motions resulting from aerodynamic forces. A 0.22 lb ballast is added to lower the center of gravity in order to minimize spurious motions. The Jimsphere's ascent rate decreases almost linearly from 17.6 ft/s at 3.3K ft to 15.1 ft/s at 50K ft.¹⁷ An AN/FPS-16, C-band, monopulse radar tracks the Jimsphere and provides position coordinates (slant range, azimuth and elevation angles) at 0.1-sec intervals.

Data reduction is performed by the Rose software program¹⁸, which processes the radar data to provide wind velocity as a function of altitude in 100-ft increments. Before transforming the data to Cartesian coordinates, the Rose program edits the radar data for outliers by monitoring the standard deviation of the first differences over 50-point segments. By computing a centered difference of the position vectors, which are averaged over 50 ft bands, wind velocity at 100 ft increments is established. This effective 100 ft averaging layer remains constant under light wind conditions when radar tracking is good. However, as the quality of the radar track deteriorates, as indicated by the standard deviation of the balloon's rise rate, Rose attempts to maintain an accuracy to about 3 ft/s by increasing the averaging layer in increments of 100 ft up to a maximum of 400 ft (Ref. 18).

3. Accuracy of Wind Profiles

The validity of turbulence/gust forcing functions derived from measured wind profiles is directly related to the accuracy of the measured wind profiles. Accuracy of the Jimsphere-Radar system in measuring horizontal wind velocity has been investigated by a number of authors. Zartarian and Thompson¹⁹ provided detail comparisons between balloon/radar systems and between data reduction methods in terms of wind profile accuracy. Luers and MacArthur²⁰ investigated the effects of variable rise rates on wind error magnitudes. Recently, Ref. 18 discussed how the effective vertical resolution is limited by radar noise and the self-induced oscillation. We shall examine the main sources of errors in the measurement system and how they affect the vertical resolution of wind profiles.

3.1 Amplitude and Phase Response

The planar equations of motion for an ascending balloon are discussed in Refs. 16 and 19. With some simplifying assumptions—lift forces are absent and the vertical wind component is zero—one can show that the balloon's steady-state horizontal velocity, \dot{x}_B , when subjected to a sinusoidal wind field defined by

$$W_x = A \sin\left(\frac{2\pi}{\lambda} \dot{z}_B t\right) \quad (1)$$

is given by

$$\dot{x}_B = AF_B \cdot A \sin\left(\frac{2\pi}{\lambda} \dot{z}_B t - \phi_B\right) \quad (2)$$

The following expressions for AF_B and ϕ_B were derived by Eckstrom,²¹

$$AF_B = \sqrt{\left[1 - \frac{\frac{L}{R} \left(\frac{2\pi R}{\lambda}\right)^2}{1 + \left(\frac{2\pi R}{\lambda}\right)^2}\right]^2 + \left[\frac{\frac{L}{R} \left(\frac{2\pi R}{\lambda}\right)}{1 + \left(\frac{2\pi R}{\lambda}\right)^2}\right]^2} \quad (3)$$

and,

$$\varphi_B = \tan^{-1} \left(\frac{\frac{L}{R} \left(\frac{2\pi R}{\lambda} \right)}{1 + \left(1 - \frac{L}{R} \right) \left(\frac{2\pi R}{\lambda} \right)^2} \right) \quad (4)$$

where,

$$L = \frac{m_B}{m_0 - m_B} \cdot \frac{\dot{z}_B^2}{g} \text{ is the lag distance,}$$

$$R = \frac{m_B + m_A}{m_0 - m_B} \cdot \frac{\dot{z}_B^2}{g} \text{ is the response distance,}$$

and the displaced mass and apparent mass are defined by,

$$m_0 = \rho_A \frac{\pi}{6} D^3, \text{ and}$$

$$m_A = 0.51m_0.$$

Plots of AF_B and φ_B are shown in Fig. 1 for altitudes of 30 kft and 45 kft. Since the Rose program provides wind velocity at 100 ft increments, Shannon's Sampling Theorem (Ref. 34) implies that we are limited to wind features with wavelengths greater than 200 ft. From Fig. 1, we see that at these wavelengths, the Jimsphere is able to "follow" the wind field with less than five percent attenuation.

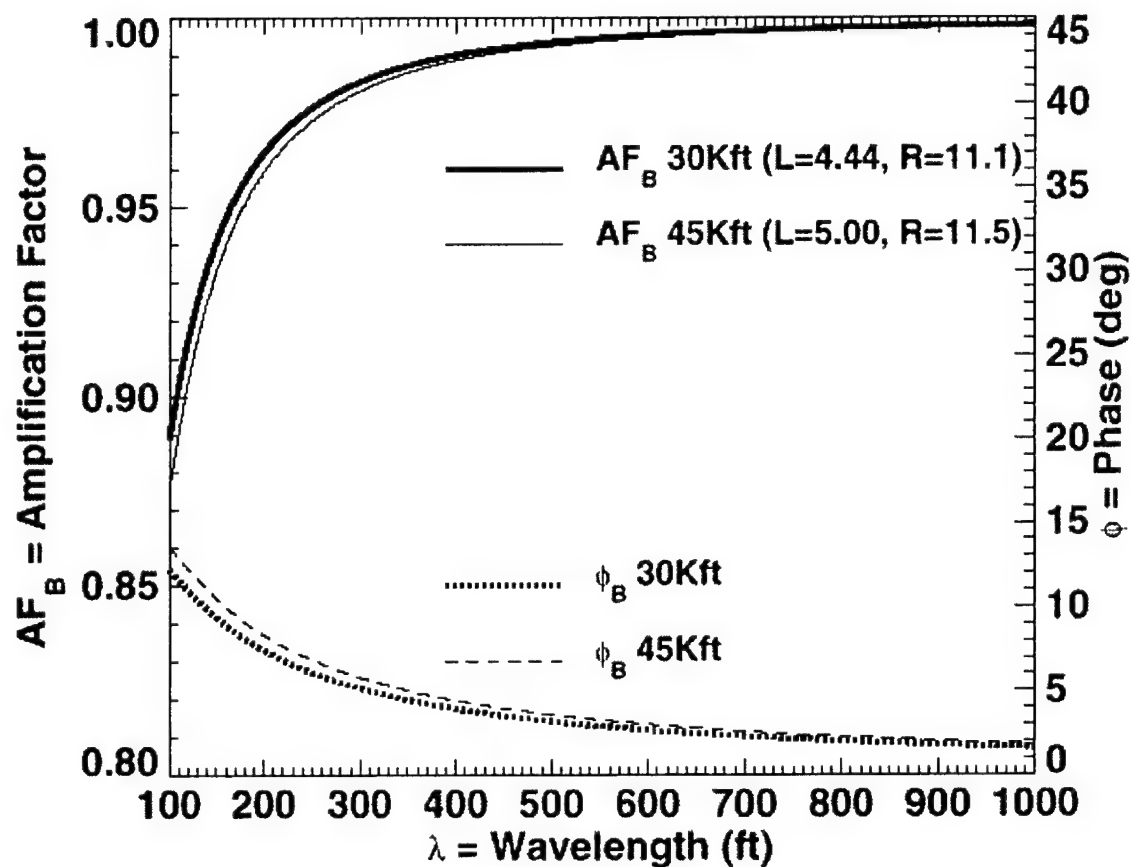


Figure 1. Amplification factor and phase response plots for Jimsphere at 30 kft and 45 kft. Attenuation is less than 5% for wavelengths greater than 200 ft. Values of L and R taken from Zartarian.¹⁹

3.2 Rose Processing Effects

Errors introduced by the Rose program can be established following an analysis²² that developed a least-squares smoothing technique for obtaining wind profiles from balloon sensor position coordinates. Assuming a sinusoidal horizontal wind field as defined by Eq. (1), Ref. 22 determined the distortion introduced by the smoothing procedure when applied to the balloon's position, given by

$$x_B = \frac{\lambda}{2\pi} (AF_B A) \cos\left(\frac{2\pi}{\lambda} h - \varphi_B\right) \quad (5)$$

where the altitude h is defined as

$$h = \dot{z}_B t.$$

For simplicity we take φ_B to be zero and assume the rise rate, \dot{z}_B , to be constant over the duration of interest. It is stated in Ref. 19 that the smoothing scheme, known as the "UDRI" method, introduces no phase distortion, and for a given averaging layer, L_{avg} , attenuates the velocity amplitude by the amplification factor

$$AF_{Rose} = \text{sinc}^2\left(\frac{L_{avg}\pi}{2\lambda}\right) \quad (6)$$

where the sinc function is defined by

$$\text{sinc}(x) \equiv \frac{\sin(x)}{x}.$$

We shall derive the above expression. Averaging x_B over the half of the averaging layer, we see that its mean position is given by,

$$\begin{aligned} \bar{x}_B(h) &= \frac{2}{L_{avg}} \int_{h-L_{avg}/4}^{h+L_{avg}/4} x_B(h') dh' \\ &= \text{sinc}\left(\frac{L_{avg}\pi}{2\lambda}\right) x_B(h). \end{aligned} \quad (7)$$

Applying a central difference to Eq. (7) using $\bar{x}_B(h \pm L_{avg}/2)$ leads to the following expression for the estimation of the balloon's velocity,

$$(\dot{x}_B)_{\text{Rose Estimate}} = \text{sinc}^2\left(\frac{L_{\text{avg}}\pi}{2\lambda}\right) \cdot (AF_B A) \sin\left(\frac{2\pi}{\lambda} h\right) \quad (8)$$

By comparing Eq. (8) with Eq. (2), we see that Rose introduces no phase shift and attenuates the velocity amplitudes by the factor defined in Eq. (6). Figure 2a presents plots of the above, using averaging layers of 100, 200, 300, and 400 ft, respectively. Observe that under nominal tracking conditions the 100 ft averaging layer causes less than five percent attenuation at wavelengths greater than 500 ft. It should be noted that earlier implementation of the Rose program used an averaging layer and altitude increments of 82 ft (Ref. 19).

In order to verify Eq. (6), the Rose program was acquired, and simulated radar data measuring sinusoidal wind profiles of known wavelengths were processed. The nominal averaging layer of 100 ft and a rise rate $\dot{z}_B = 15.6$ ft/s corresponding to an altitude of 35K ft were used. The simulated results are shown in Fig. 2b, which agree well with the analytical expression presented above.

The extent to which the Jimsphere's response characteristics and the Rose program's smoothing scheme distort the true wind velocity can now be quantified for wavelengths greater than 500 ft. Since Rose introduces no phase shifts, we have from the preceding discussion that phase distortion is less than one percent, all of which is produced by the balloon's ability to follow the wind. Whereas phase is additive, amplification factors are multiplicative, therefore implying that the product, $AF_B \cdot AF_{\text{Rose}}$, indicates the combined attenuation effects of the balloon's dynamics and the data reduction method. Figure 3 shows that, for the nominal averaging layer of 100 ft, the combined attenuation effect of the Jimsphere, and the Rose program is less than five percent at wavelengths greater than 500 ft.

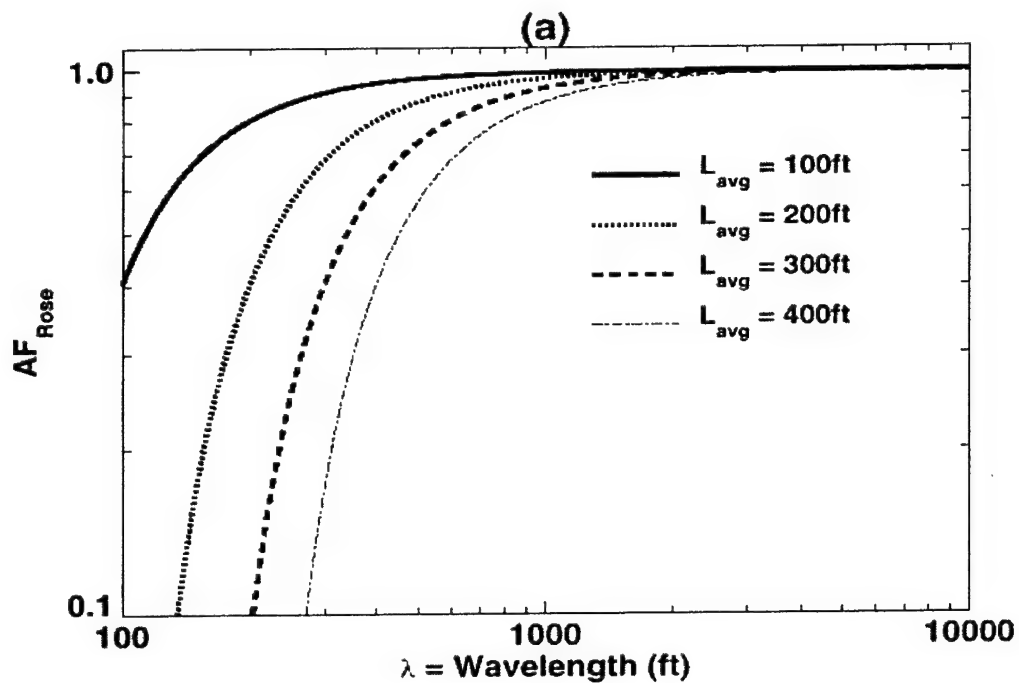


Figure 2a. AF_{Rose} at various averaging layer lengths. The nominal averaging layer of 100 ft produces less than 5% attenuation for $\lambda \geq 500$ ft.

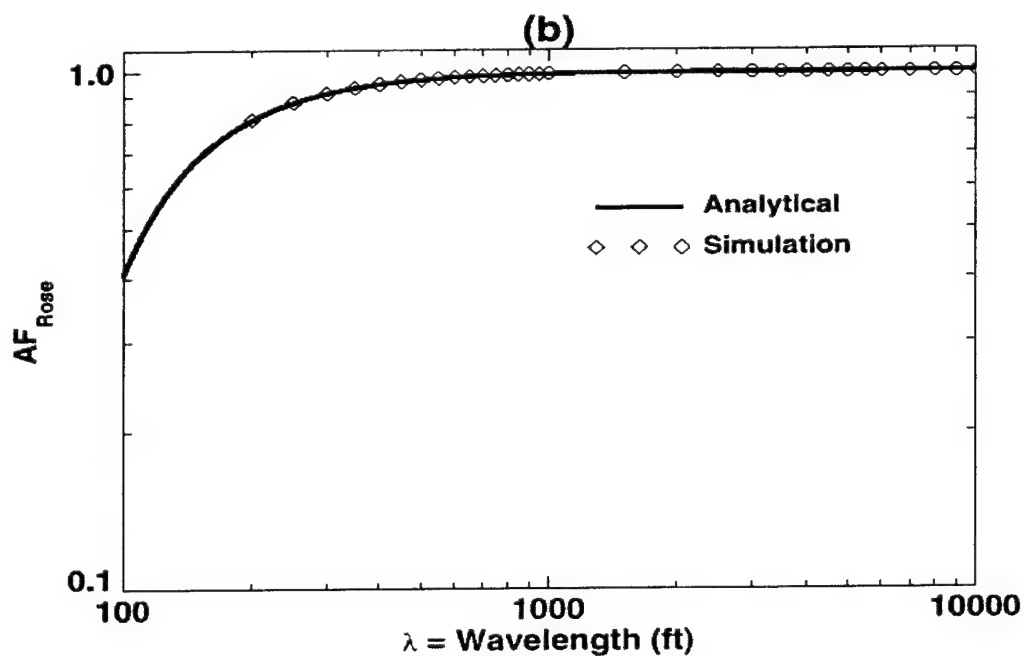


Figure 2 b. Verifying AF_{Rose} by comparing to attenuation factors from Rose program simulation using sinusoidal wind fields at various wavelengths.

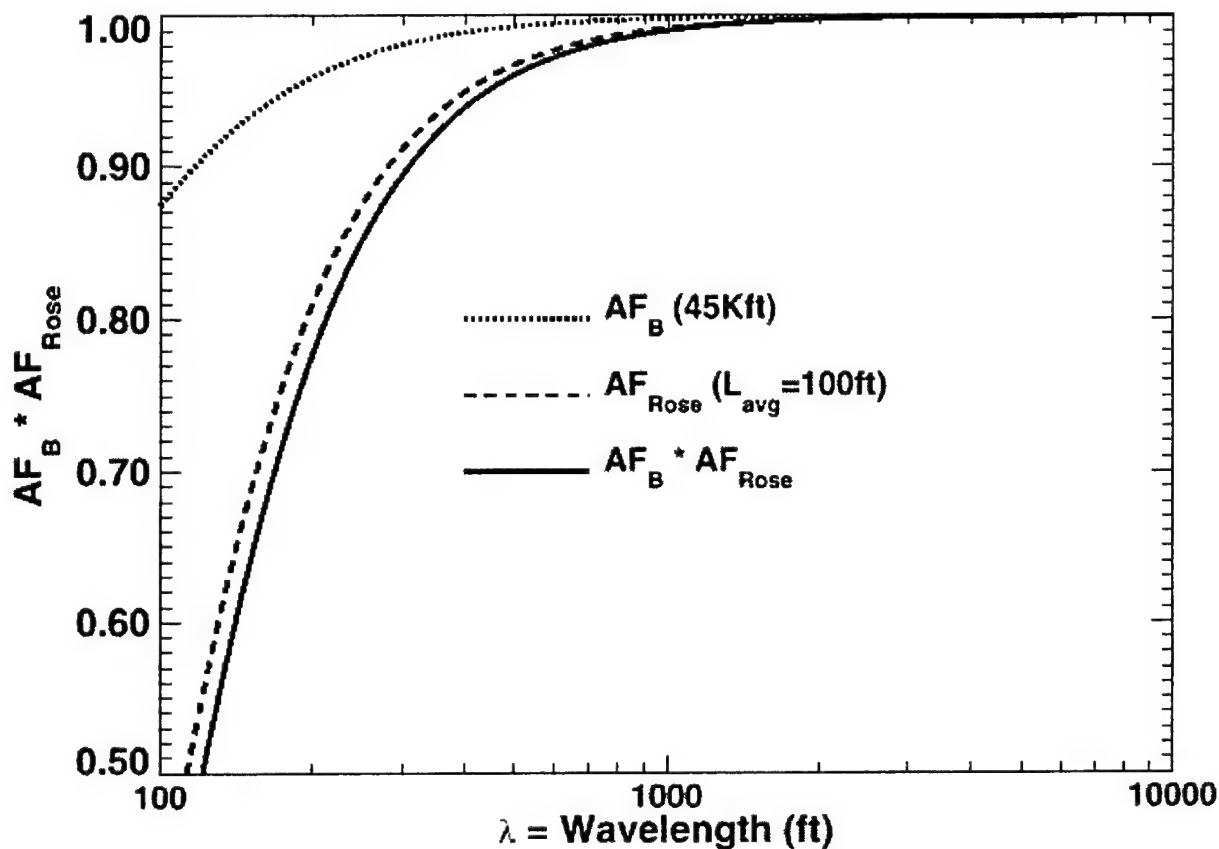


Figure 3. Combined amplification factor from Jimsphere and Rose program is less than 5% for >500 ft.

3.3 Self-Induced Oscillations and Aliasing Errors

It is well known^{19,23} that the Jimsphere will exhibit lateral self-induced motion due to aerodynamic lift forces which depend on the Reynolds number,

$$Re = \frac{|\dot{z}_B| D_B}{\nu}$$

At subcritical Reynolds number, i.e., $Re \leq 2.5 \times 10^5$, which occurs at altitudes greater than 35K ft, the Jimsphere will execute a regular 0.21 Hz spiral motion.²³ Unlike smooth balloon sensors whose lateral motions become erratic at supercritical Reynolds numbers, $Re > 2.5 \times 10^5$, the roughness elements of the Jimsphere allow it to maintain its spiral motion throughout its ascent.

Reference 23 determined the velocity's amplitude to be proportional to \dot{z}_B , and that it decreased linearly with altitude from 7.9 ft/s near the surface to 3.3 ft/s at 49K ft. The Rose program does not remove the effects of the self-induced oscillations. Therefore, because of aliasing, this oscillation would manifest

itself as oscillations with wavelengths in the neighborhood of 300 ft. Figure 4 shows the power spectral density (PSD) function of an atypical Jimsphere wind profile with a strong spectral peak due to the self-induced oscillations. A 0.21 Hz oscillation implies that the Jimsphere completes one cycle every 4.76 s. Therefore, the variation in the Jimsphere's rise rate, corresponds to variations in wavelengths of about 82 ft near the surface to 72 ft at 50K ft. Figure 5 shows how the Rose 100 ft sampling aliases these to wavelengths between 450-250 ft. Reference 18 verified the effects of aliasing and quantified these errors by applying the Rose program to radar data for simulated balloon releases. With the nominal averaging layer of 100 ft, their results indicate aliasing errors of 1.5 ft/s at 15K ft decreasing almost linearly to 0.15 ft/s at 50K ft.

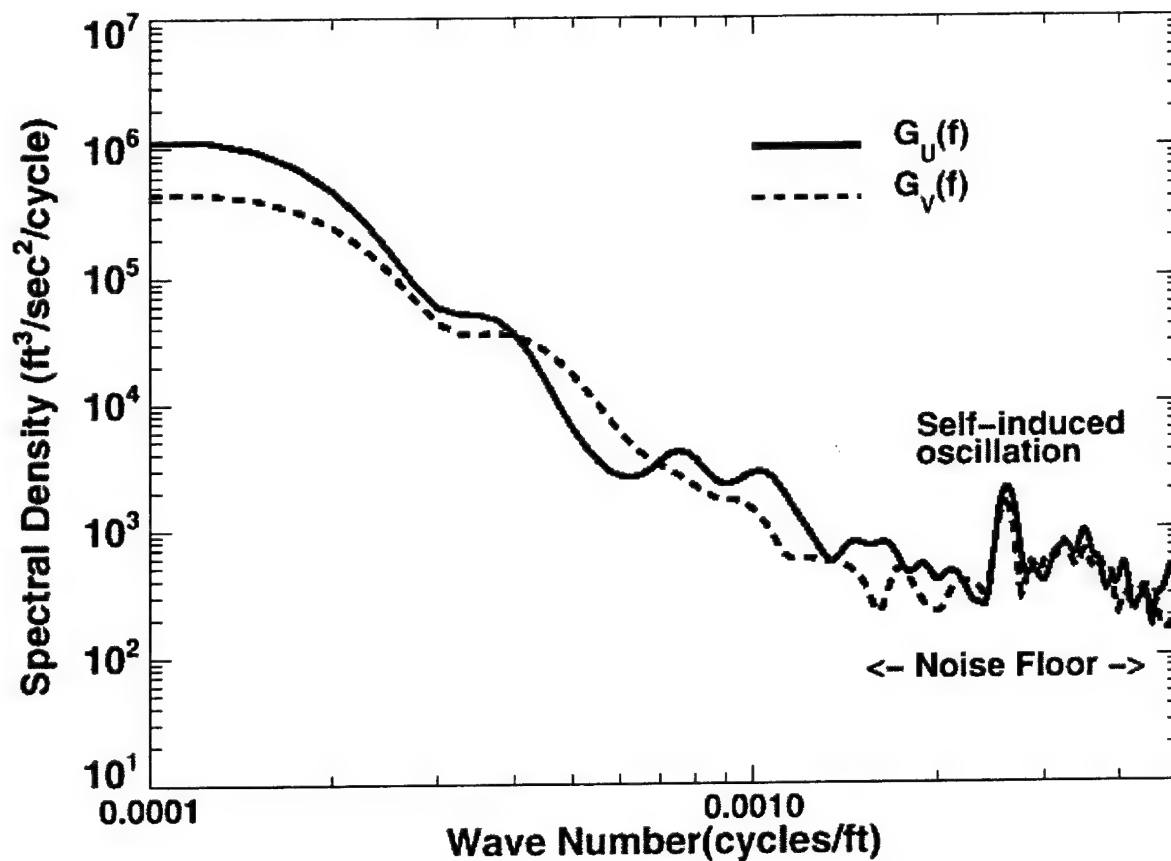


Figure 4. Power Spectral Density of U and V wind components of a typical Jimsphere wind profile shows the self induced oscillation and the noise floor.

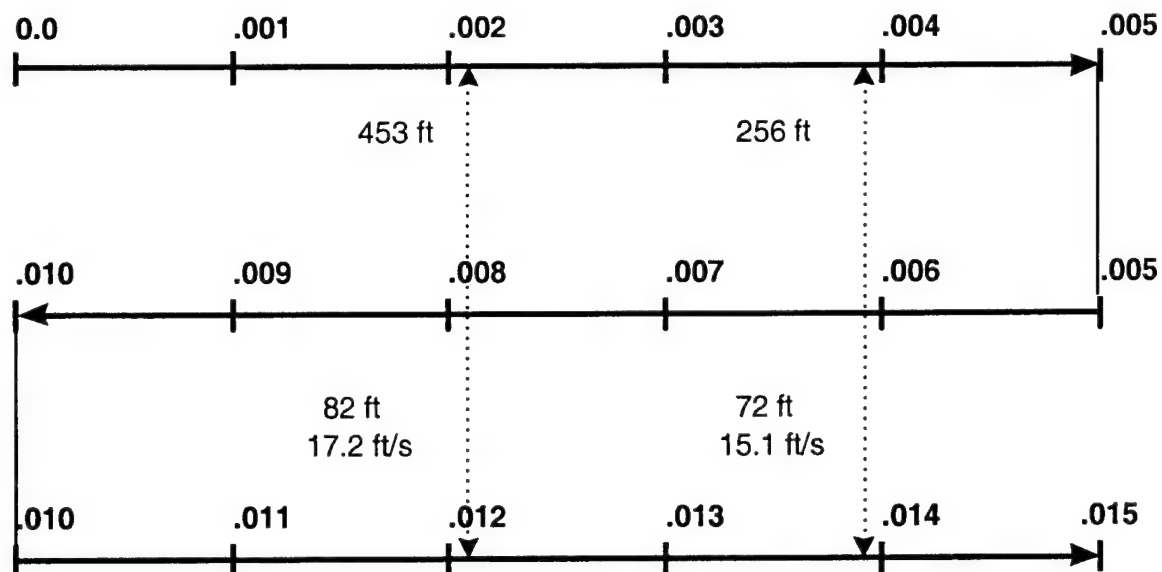


Figure 5. Nyquist folding diagram showing how self-induced oscillations at 72-82 ft are aliased to wavelengths at 450-250 ft due to the Rose program's 100-ft sampling.

3.4 Radar Errors

The performance of the AN/FPS-16 radar in tracking the Jimsphere has been examined by a number of investigators.^{19,24,25,26} Basically, radar errors are classified as either bias errors or noise errors. In general, bias errors do not contribute significantly to wind measurement errors since they are effectively removed by the central differencing done within the Rose program. On the other hand, noise error in position persists into the velocity estimate which produces a "noise floor" in the wind's PSD (Fig. 4).

Using 33 dual-tracked Jimspheres, Ref. 18 computed the root mean square vector difference, which was then scaled by $1/\sqrt{2}$ to account for the noise contributions from the two radars. The result indicates that the radar noise error increases with slant range, typically ranging from 1 ft/s at low altitudes to 2 ft/s above 45K ft. Additionally, Ref. 18 concluded that the wavelength at which the noise floor becomes apparent effectively limits vertical resolution to approximately 500-650 ft under good tracking conditions, and 800-1000 ft at longer slant ranges.

4. Validity of Wind-Derived Forcing Functions

From the above discussion, it is reasonable to conclude that the Jimsphere wind profiles, at the altitudes of interest (30K-50K ft) for this study contain accurate wind velocity data at wavelengths longer than 500 ft. At these wavelengths, the attenuation and phase errors introduced by the Jimsphere's response characteristics and the Rose program are small. Although, aliasing of the self-induced oscillations limits the accuracy of the wind to wavelengths larger than 500 ft, these errors are reduced at the higher altitudes of interest to less than 1 ft/s.

Perhaps the greatest source of error which degrades the accuracy of measurements is radar noise. In general, these errors limit effective vertical resolution to approximately 500 ft. However, under inclement weather, where tracking conditions are poor, radar noise will contaminate wind features at scales as large as 1000 ft with RMS errors of about 2 ft/s. For these measurements, we shall show that a simple noise-reducing filter extends the usable spectrum to include wind features as small as 500 ft.

The accuracy in measured winds, therefore, makes turbulence/gust forcing functions derived from these wind profiles applicable to loads analyses of launch vehicles whose lower modes of vibration correspond to wavelengths longer than 500 ft. Currently, launch vehicles that are classified as medium-lift launch vehicles (MLV) and heavy-lift launch vehicles (HLV) fall into this category. The forcing functions derived herein should not be used on systems whose critical loads are defined by the shorter wavelength components of atmospheric turbulence; i.e., less than 500 ft. Many small launch vehicles and most space vehicles fall into this category.

5. Wind Database Description

A database consisting of 1093 WR and 1197 ER Jimsphere wind profiles dating from 1964 to 1997 was used in the derivation of the forcing functions. Most of the wind data collected during this period were associated with day-of-launch operations. Figure 6 shows the monthly distributions of the wind profiles. As mentioned earlier, some of the Jimsphere wind radar data were reduced, using an averaging layer and altitude increment of 82 ft, rather than the current standard of 100 ft. In general, WR winds prior to 1989 and ER winds prior to 1987 were processed using 82 ft. The yearly distributions are shown in Fig. 7.

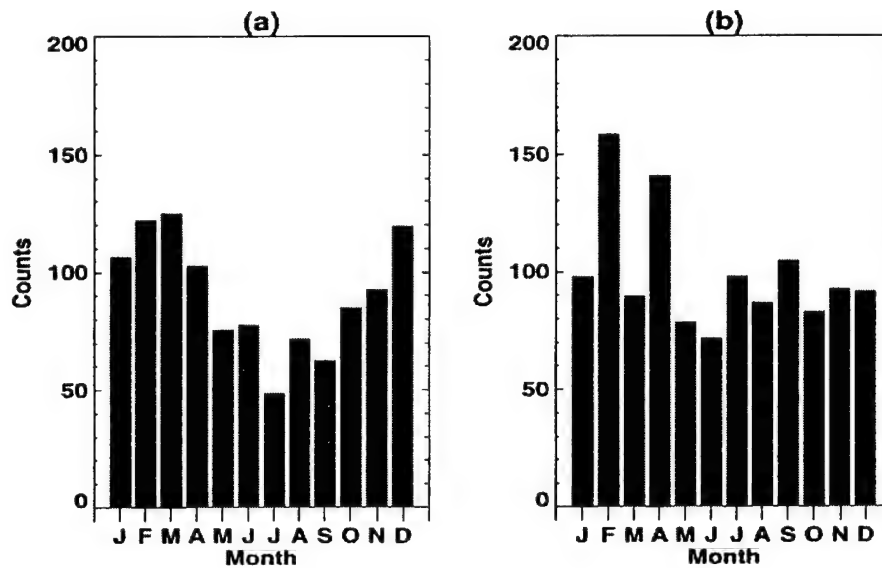


Figure 6. Monthly distributions of WR (a) and ER (b) Jimsphere wind profiles.

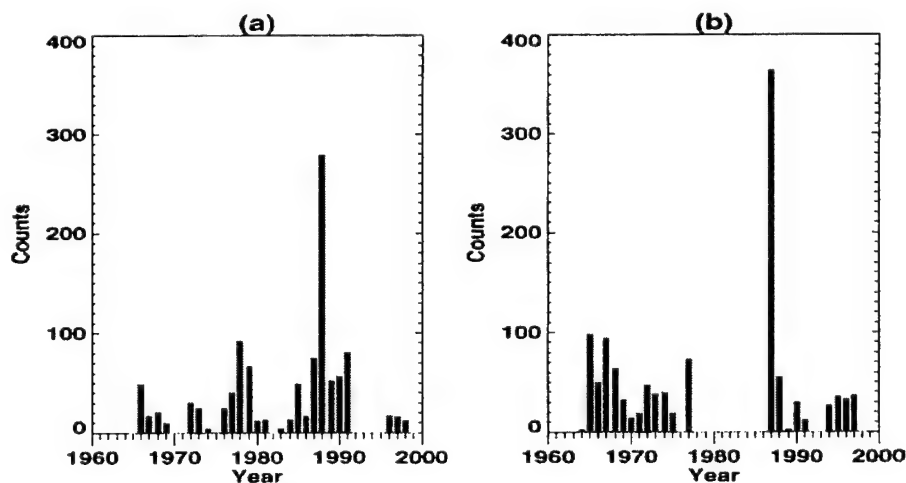


Figure 7. Yearly distributions of Jimsphere wind profiles for WR (a) and ER (b).

6. Forcing Functions Derivation

Figure 8 illustrates the process used to derive forcing functions from two wind profiles. Figure 8a shows a sample wind magnitude profile restricted to a 6000 ft altitude band. A moving two-point average was applied to remove the noise floor. In Figure 8b, shown in dashed-line, is the trend which the high-pass filtering removed to yield the small-scale and rapidly changing wind features. Figure 8c shows the flattop tapering performed on the resulting filtered data to minimize step response transients. The final turbulent component of the wind to be used as the forcing function is shown in Fig. 8d. The following subsections describe in further detail each of the above steps.

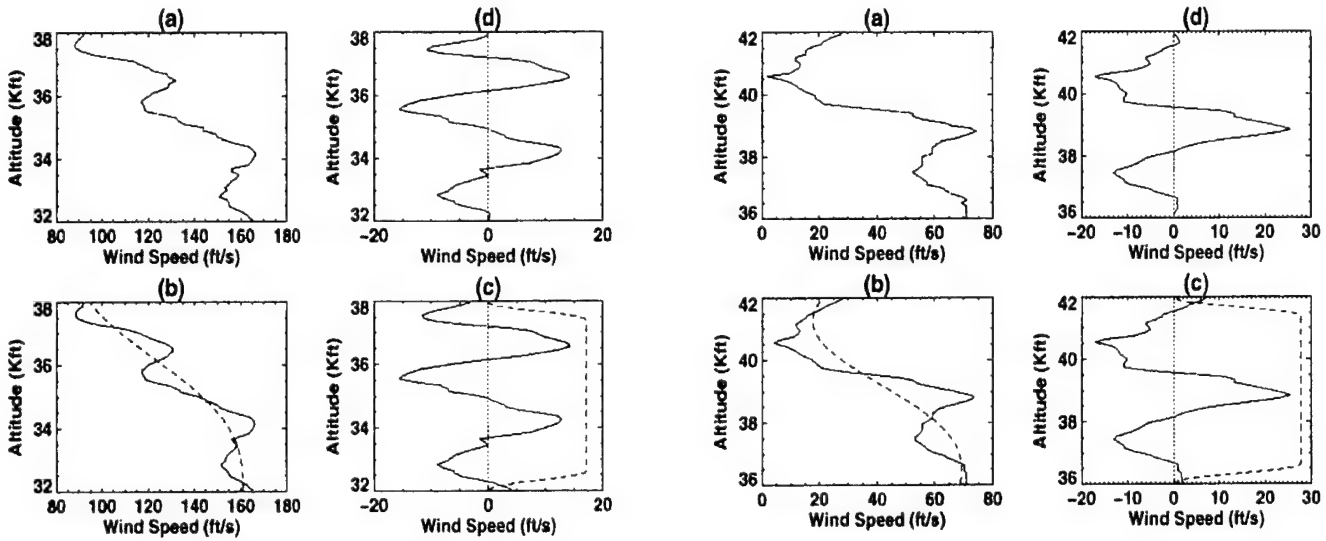


Figure 8. Two examples of method used to derive forcing functions: a) Typical unprocessed wind magnitude for 6000 ft altitude band; b) Two-point smoothing to remove the noise floor and detrending to extract small-scale features shown in c); c) Turbulence that is tapered; d) Resulting turbulent wind component to be used in launch vehicle gust loads analysis.

6.1 Removal of Noise Floor

It was previously stated that the radar noise accounts for the leveling of the wind's PSD at wavelengths near 500-1000 ft. That this noise floor is not indicative of wind features is based upon numerous investigations which show that despite seasonal, climatic, and topographical differences, the wind's vertical wavenumber PSD obeys a power law of the form,

$$G(f) \propto \frac{\omega^2}{f^\gamma},$$

where f and ω represent the vertical wavenumber and the “buoyancy frequency,” respectively. VanZandt²⁷ was the first to describe this, using $\gamma = 2.4$, in terms of a “universal” spectrum of atmospheric buoyancy waves.^{28,29} References 28 and 29 modeled similar spectra observed in the ocean.

Dewan and Good³⁰ later conjectured that the PSD amplitudes at any given wavenumber are limited by its saturation value, likely due to convective instability. Their theory leads to a PSD power law with $2.5 \leq \gamma \leq 3$. Moreover, they showed that simple dimensional analysis yields $\gamma = 3$ since the PSD should scale as $\text{Hz}^2/(\text{cycles/ft})^3$. Reference 31 advanced a more general theory arguing that the spectral amplitude should decrease as $1/f^3$, resulting from the superposition of individually saturated gravity waves.

Further evidence that the noise floor is directly related to the radar noise is obtained from dual tracking experiments.^{32,18} Reference 18 computed cross-spectral densities (CSD) for 33 dual-tracked Jimsphere wind profiles. Their results showed that except for the presence of the aliased self-induced oscillation, the CSD amplitudes conform to the power law and, moreover, confirmed the hypothesis that the noise floor is due to radar noise which is uncorrelated to the true wind profile.

Figure 9 shows that the ensemble averages of wind magnitude PSDs from WR and ER obey the power law with $\gamma \approx 2.7$. Each PSD was computed via the method described in Bendat and Piersol³³ using 10K ft discrete Fourier Transforms, with 50 percent overlap, and a Hanning data window. The onset of the noise floor at wavelengths smaller than 500 ft implies that we can, in general, expect adequate resolution at this scale. Additionally, we note that WR's PSD is greater than that of ER, thereby implying that turbulence from WR tends to be more severe than ER.

Since the noise floor is not a measure of the wind, we need to minimize its contribution to the forcing functions by low-pass filtering. Another reason for minimizing the noise floor is to ensure that the Monte Carlo gust loads analysis approach is applicable to medium lift launch vehicles, which typically require wavelengths starting in the neighborhood of 800 ft. This requirement is generally met for light winds when radar tracking is good. Therefore, this concern applies mainly to the filtering of wind profiles which were measured under strong wind conditions, when radar noise can corrupt wind components with wavelengths less than 1000 ft. The criterion for selecting a low-pass filter, therefore, was that it should remove the noise so that the resulting spectrum conforms to the power law.

An optimal filter (or Wiener filter) is generally used to remove noise from a waveform with a known PSD.^{34,35} This approach was tried initially but later abandoned. The method assumes stationarity and that the true wind, W , is corrupted by uncorrelated noise, n , thereby giving a measured wind of the form,

$$\hat{W} = W + n.$$

The optimal filter's frequency response could then be shown equal to

$$H_{opt}(f) = \frac{G_W(f)}{G_{\hat{W}}(f)},$$

where G_W and $G_{\hat{W}}$ are the PSDs corresponding to W and \hat{W} , respectively. Since G_W is unknown, it was replaced by a power law defined by a least square fit over the interval $0.000125 \leq f \leq 0.00125$, leading to,

$$H_{opt}(f) \approx \frac{C/f^\gamma}{G_{\hat{W}}(f)},$$

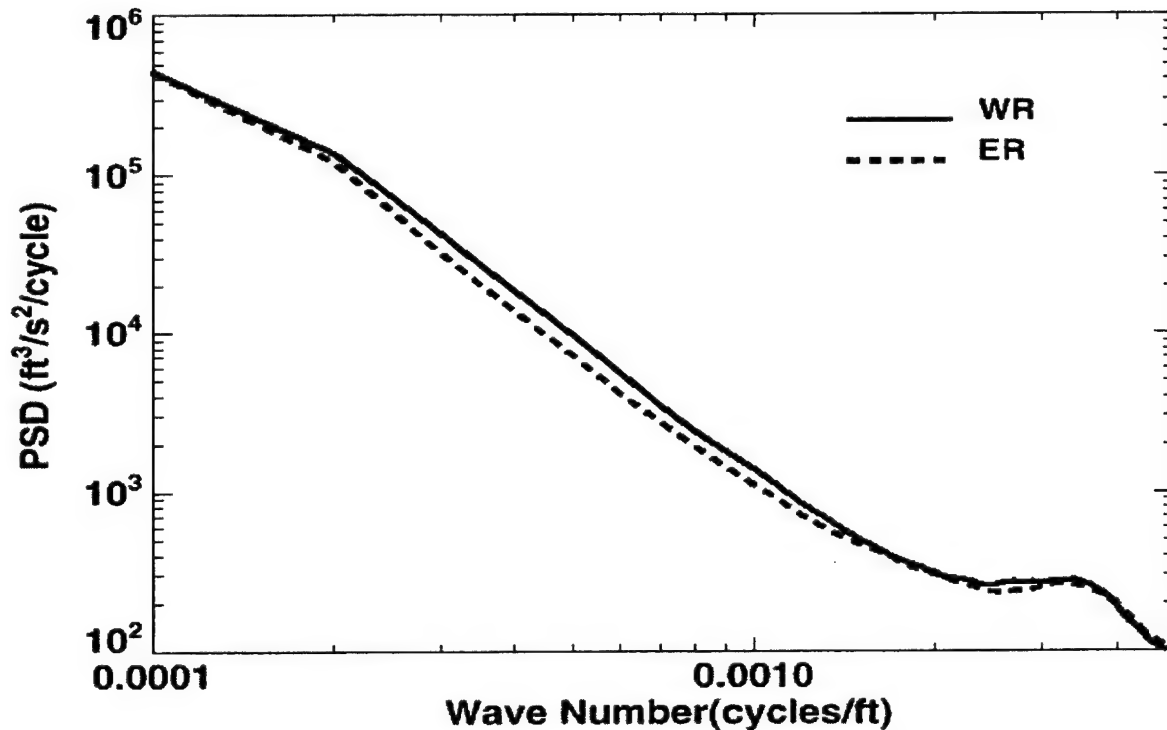


Figure 9. Ensemble averages of wind magnitude PSDs from WR and ER obeying the power law with $\gamma \approx 2.7$. The averages imply that we can expect adequate resolutions at wavelengths larger than 500 ft. That WR has a larger spectrum than ER seems to imply that turbulence from WR tends to be more severe than ER.

with, C a constant, defined by the fit. PSDs were computed for all WR and ER winds and the power law fitted to each spectrum. The resulting γ varied between 2 and 3.5 and depended upon the spectral estimation and the wavenumber interval used for the fit. Moreover, it was found that, in general, these filters did not effectively remove the noise floor, and to do so required "tuning" each filter by increasing γ . Because of this lack of robustness, and the fact that each wind would have its own unique filter, another filtering scheme was sought.

The increase in γ , needed to remove the noise floor, indicates that a faster decay in the filter's amplitude response was needed. This led to considering filters having a zero at the Nyquist frequency. A two-point moving average which averages consecutive data points is the simplest of all finite-impulse-response filters with this property, and was, therefore, selected for the purpose of removing the noise floor. Since wind profiles are reported at 100 ft increments, the resulting filtered data were also shifted forward by 50 ft to avoid any phase shifting.

Figure 10a shows a typical wind profile before and after filtering. The “noise” component which was removed by the filtering procedure is shown in Fig. 10b, which tends to increase with slant range, as does radar noise. Figure 11 compares the PSD of filtered and unfiltered data. The unfiltered data have a noise floor beginning at 1000 ft. We see that based on adherence to the power law, this filtering scheme extends the usable spectrum to wavelengths as small as 500 ft. Also shown in Fig. 11 is the PSD of the noise component which has the characteristic flat spectrum.

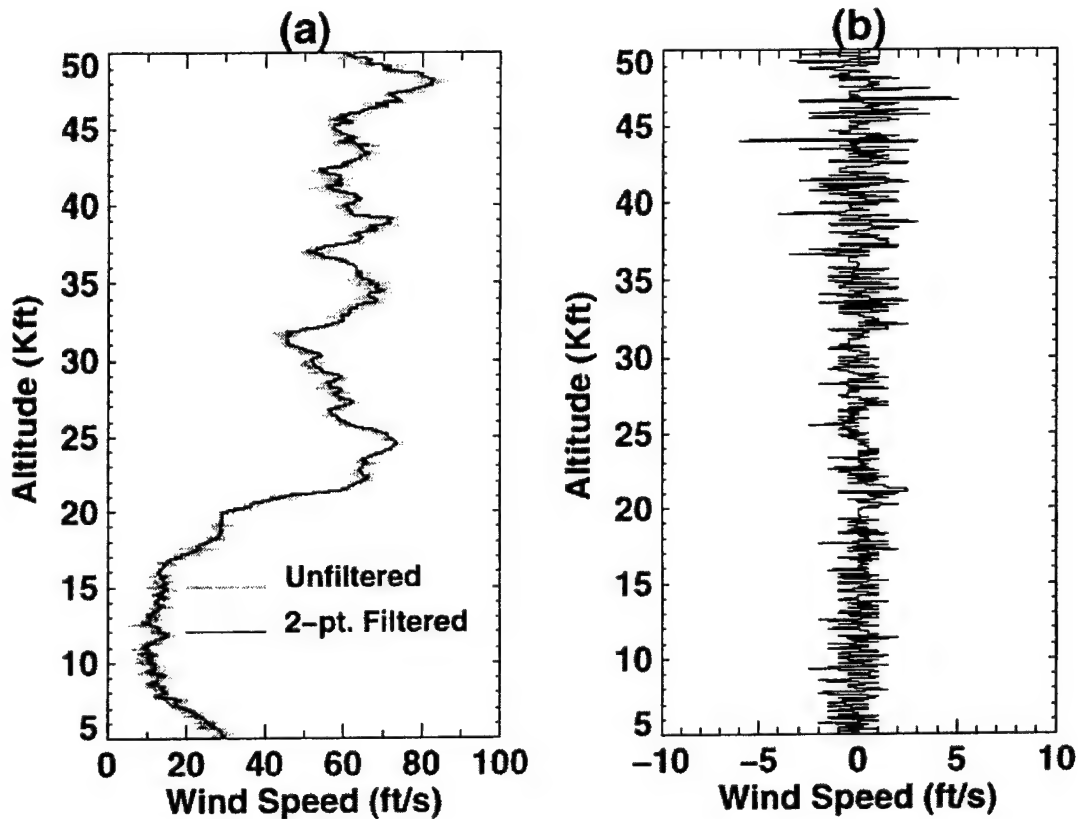


Figure 10. a) Comparison of unfiltered and 2-point filtered wind profile;
b) Noise removed by the filtering process.

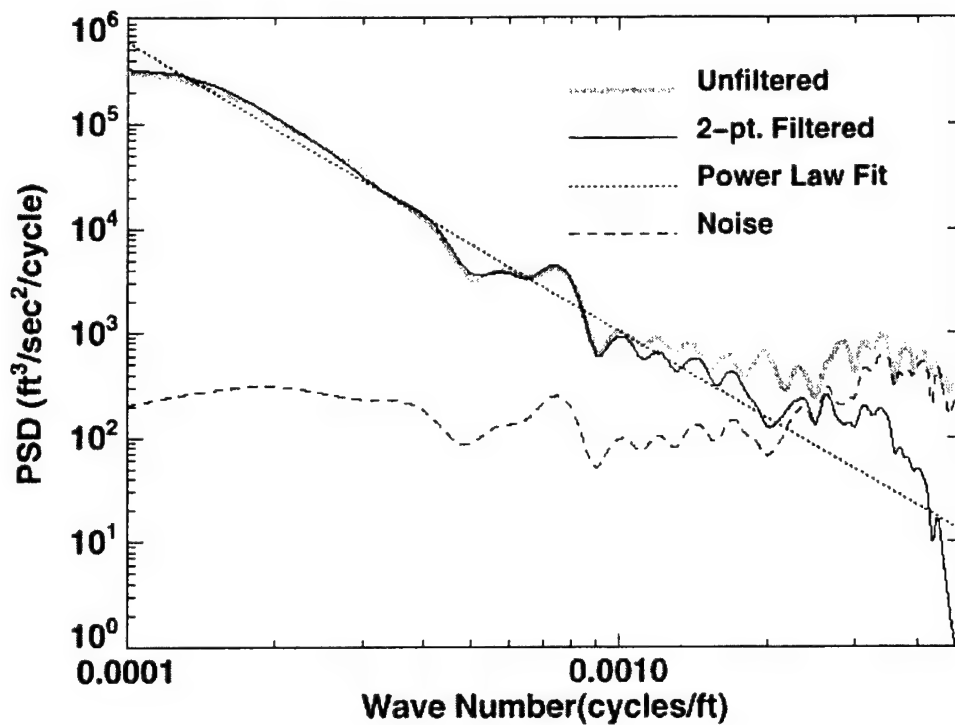


Figure 11. Two-point filtering removes noise floor having a flat spectrum and extends the usable spectrum to include wavelengths ≥ 500 ft.

6.2 Extraction of Turbulent Wind Features

Extraction of the small-scale turbulent component of the wind was accomplished by way of a high-pass filter. For the gust forcing functions, the filter's corner wavelength, λ_G , was based on earlier work³⁶ which analyzed hundreds of wind pairs and established a wavelength boundary, λ_B , where wind features smaller than it no longer remain coherent after a given length of time. The component of the wind which consisted of these small-scale and short-duration wind features was referred to in Ref. 36 as the rapidly-varying, turbulent component of the wind. Using wind pairs from the database, Ref. 36 estimated the mean wavelengths which spectrally separate the slowly-varying and turbulent wind components for wind pairs 30, 60, 90, and 120 minutes apart. A curve fit was then applied to this data that led to the simple empirical formula relating λ_B as a function of the time, ΔT , between wind pairs:

$$\lambda_B = 460\sqrt{\Delta T}.$$

The above formula suggests that as ΔT increases, so does the lack of wind persistence at longer wavelengths, which needs to be accounted for in a gust analysis. Because of the variation about the estimated λ_B , and to ensure sufficient conservatism in the forcing functions, λ_G was defined by λ_B plus an estimated one standard deviation, which also depended upon ΔT . For the purpose of this study, the standard deviations were estimated from the "normal" regions of the wavelength histograms presented in Ref. 36 and resulted in three filter corner wavelengths,

$\lambda_G = 3300, 4200, \text{ and } 4700 \text{ ft}$

corresponding to ΔT of 30, 45, and 60 minutes, respectively.

A 16-pole Butterworth high-pass filter was applied where the filter's half-power cutoff frequency was selected so that the attenuation of wind features smaller than λ_G was less than one percent. Moreover, the high-pass filter was applied forward and then backward to eliminate phase shifts. This procedure was applied using the three-filter corner wavelengths, λ_G .

The PSD curves shown in Fig. 12 illustrate, spectrally, the effect of the high-pass filtering on the wind profiles using the three-filter corner wavelengths. The corresponding effects of filtering in the altitude domain are shown in Figs. 13-15. In these examples, the 2-pt smoothed wind magnitude profile shown in Fig. 10a was high-pass filtered at the corner frequencies stated above. The figures show how increases in the time, ΔT , for which the forcing functions are valid, result in additional longer wavelength wind features in the gust forcing functions.

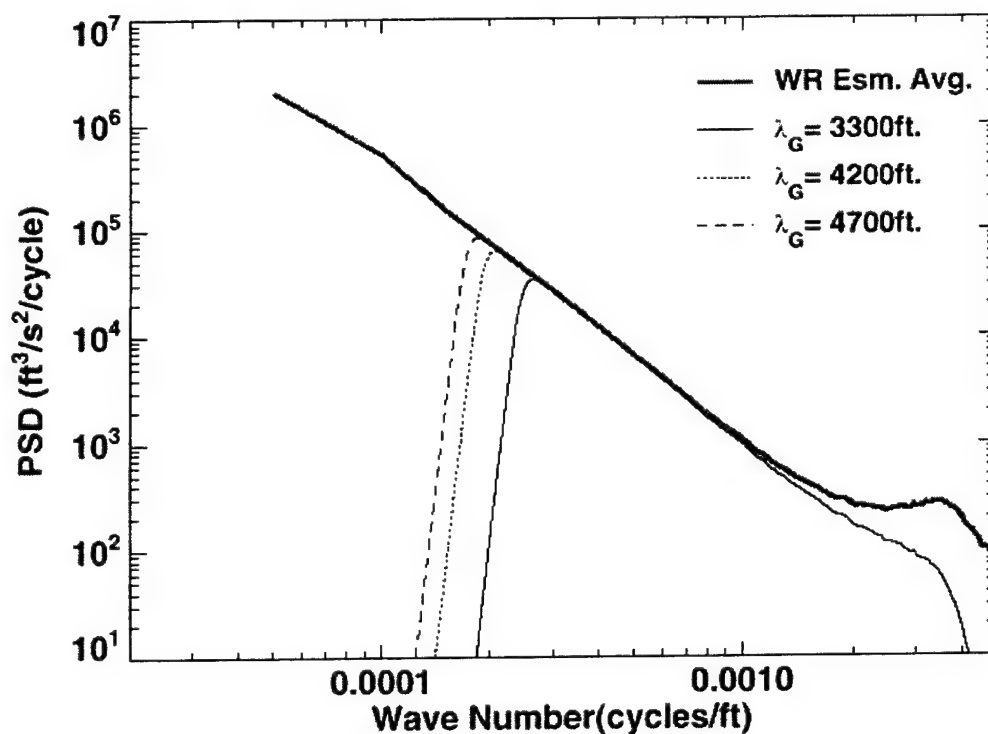


Figure 12. Ensemble averages of filtered wind PSDs for $\lambda_G = 3300, 4200, \text{ and } 4700 \text{ ft}$.

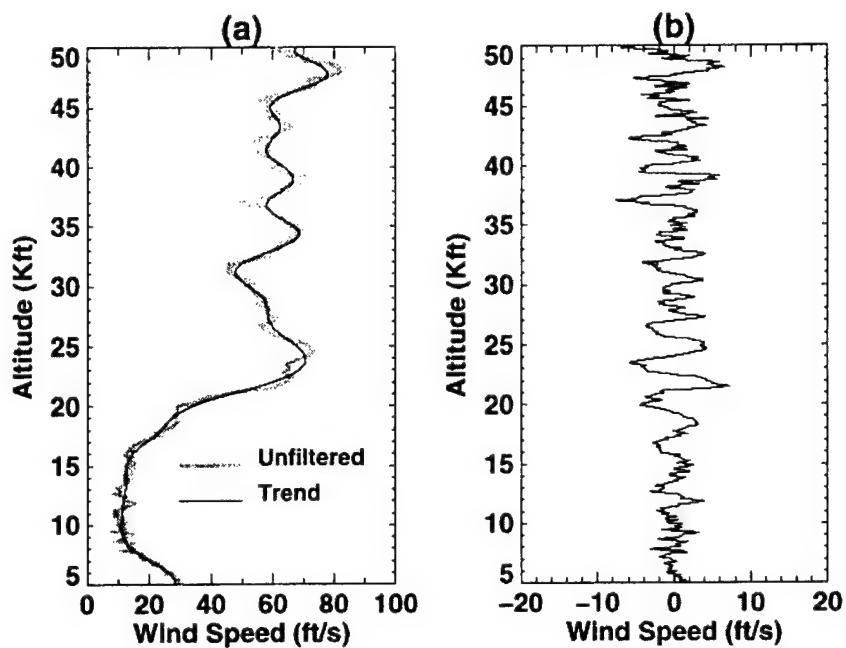


Figure 13. a) Two-point smoothed wind and trend removed for $\lambda_c = 3300$ ft.;
b) High-passed filtered wind profile.

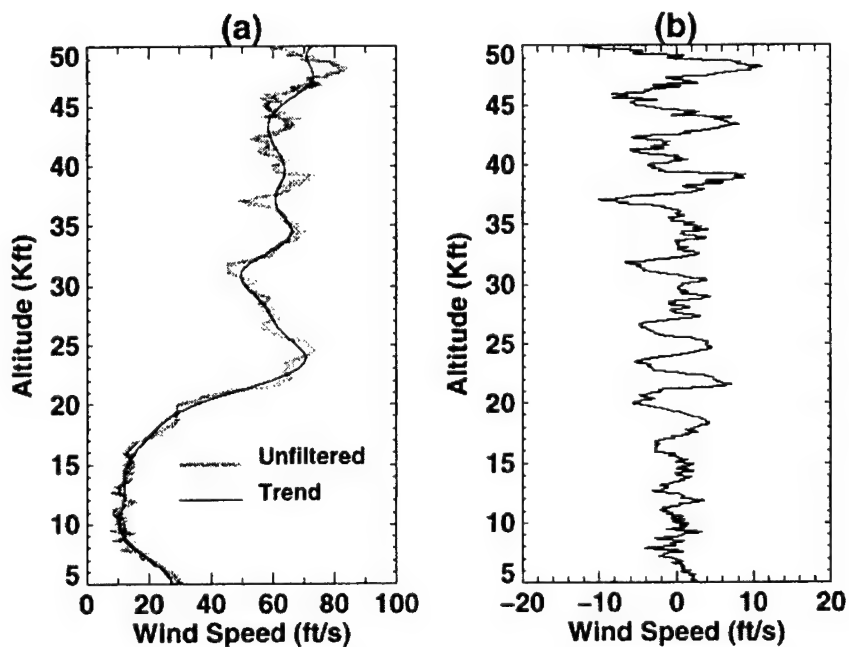


Figure 14. a) Two-point smoothed wind and trend removed for $\lambda_c = 4200$ ft.;
b) High-passed filtered wind profile.

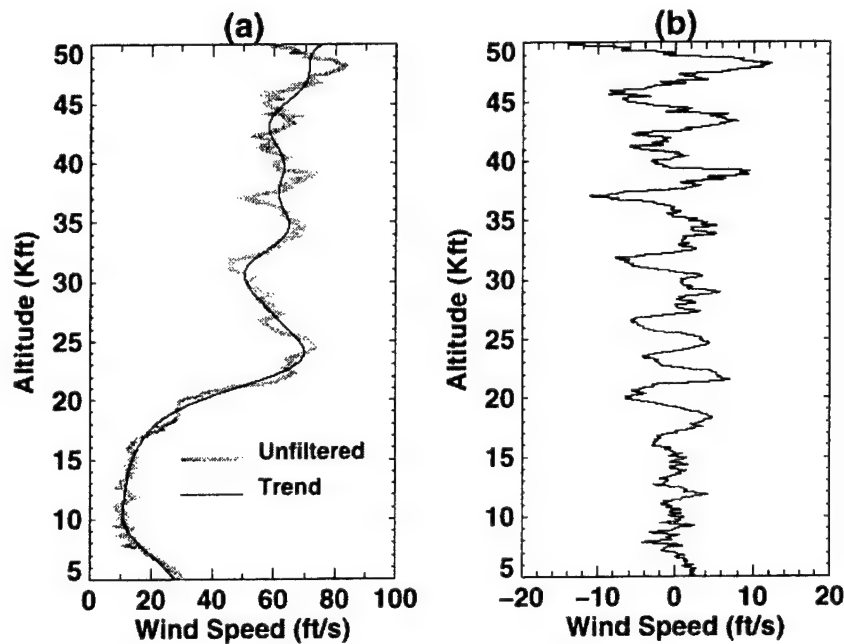


Figure 15. a) Two-point smoothed wind and trend removed for $\lambda_G = 4700$ ft.;
b) High-passed filtered wind profile.

6.3 Restriction to 6000-ft Bands

Because of the variation in the structural dynamic properties, aerodynamic characteristics, and the launch vehicle's velocity, and the desire to have altitude consistent gust loads, the gust analysis (see Ref. 15) required each filtered wind profile to be restricted to an altitude band of 6000 ft. To minimize step responses during the gust loads simulations, a flattop window having a ten percent cosine taper at each end was used (Fig. 8c). Turbulence/gust forcing functions were developed for four overlapping 6000 ft bands covering an altitude range of 32,000-48,000 ft; i.e., 32-38, 36-42, 38-44 and 42-48K ft altitude bands. Thus, for each Range, λ_G , and altitude band, a total of 24 sets, each containing over 1000 forcing functions, was developed.

6.4 Screening of Wind Data Using a Shear Criterion

Most of the Jimsphere wind data were from day-of-launch balloons and hence have gone through some form of quality control. However, a few profiles exhibited questionable features and were generally associated with older data in which the data quality information was lost, and therefore, had to be either accepted or rejected based on engineering judgment.

The screening criterion selected was the wind shear value. Wind shear is defined as dW/dh , where dW is the speed change for the altitude difference, dh . A shear value greater than 0.1 sec^{-1} is unlikely. Generally, shear values from measured wind profiles that exceed 0.1 sec^{-1} are noise driven and are not caused by actual wind shear features. If the high-frequency noise is removed, as was done by the 2-pt filtering, then it is unlikely that shears would exceed 0.1 sec^{-1} . Therefore, the screening of wind data using a shear criterion of 0.1 sec^{-1} was used on the filtered winds. A typical wind profile that was

rejected on this basis is shown in Fig. 16. Furthermore, each profile was visually reviewed to establish its reasonableness.

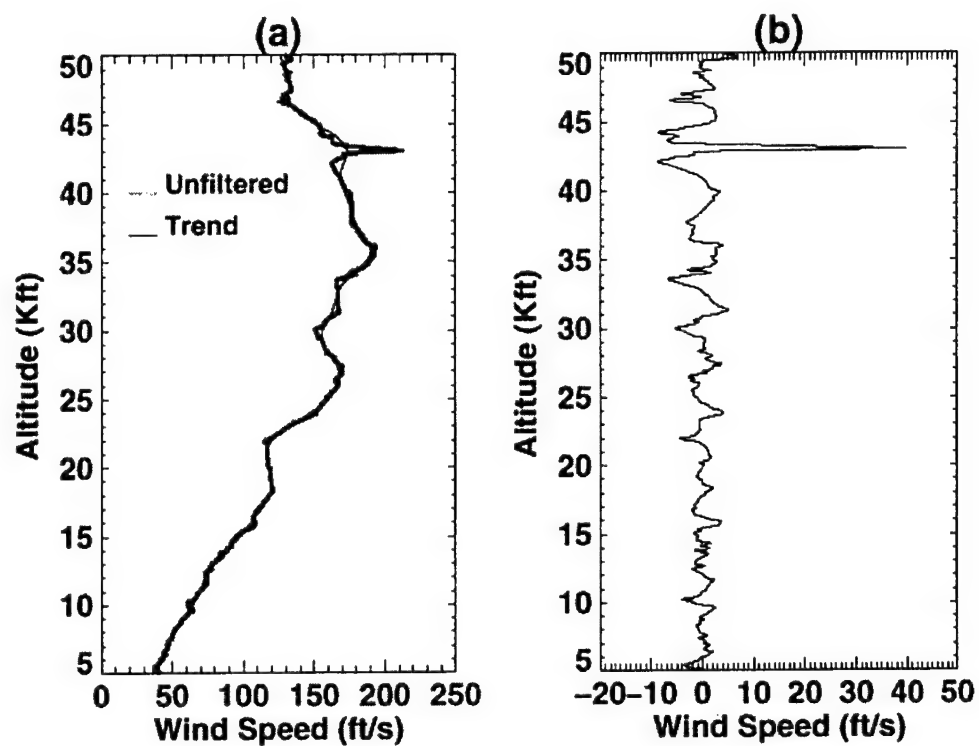


Figure 16. Wind profile with $dW/dh|_{\max} \approx 0.28 \text{ sec}^{-1}$ and failing the shear criteria. ($\lambda_G = 3300 \text{ ft}$).

7. Results

Comparison plots of WR forcing functions which were derived using various λ_G values are shown in Figs. 17-19 for three representative profiles. These figures indicate that there is a wide variation in forcing function profiles, which do not resemble the synthetic profiles used in past gust analyses.

The methodology described herein was implemented in a computer program that generates a set of gust forcing functions from the wind database for a given launch range, filter corner wavelength λ_G , and altitude band. The program was used to develop 24 sets of forcing functions that were used in the Monte Carlo gust analysis described in Ref. 15.

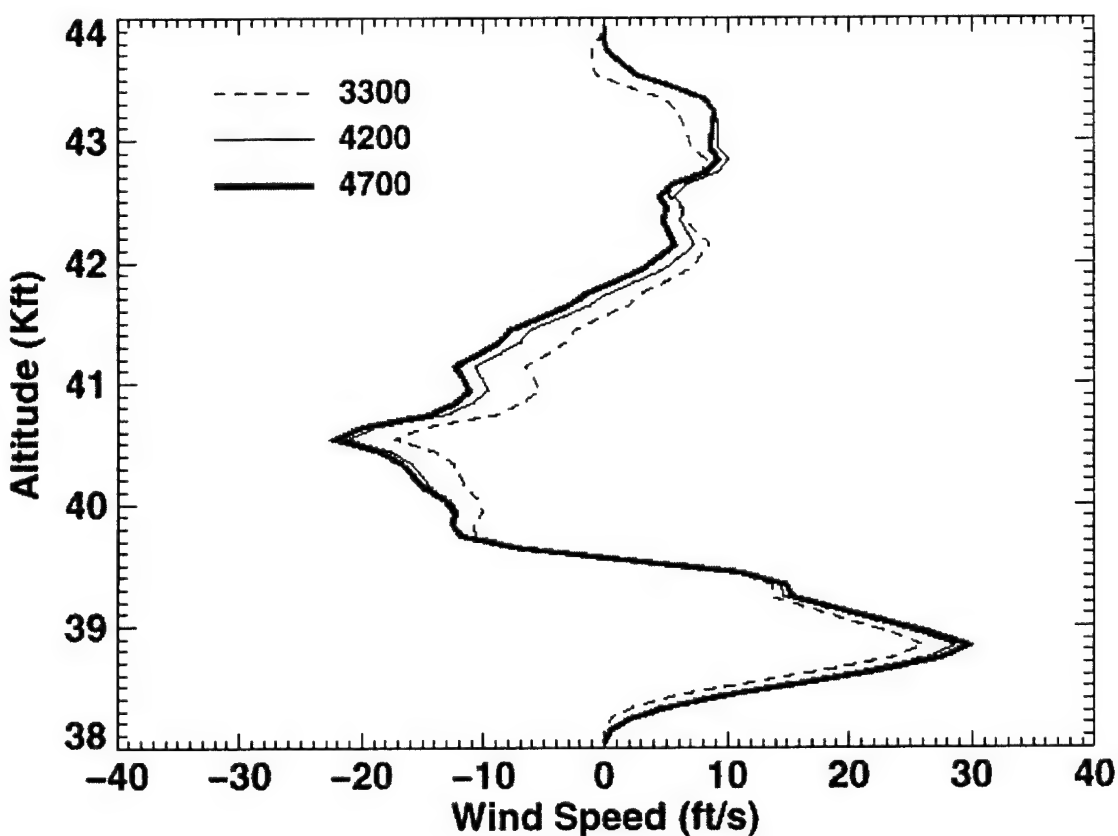


Figure 17. Forcing function comparisons using different λ_G . Taken from Jimsphere profile WR 02-12-72 08:59Z.

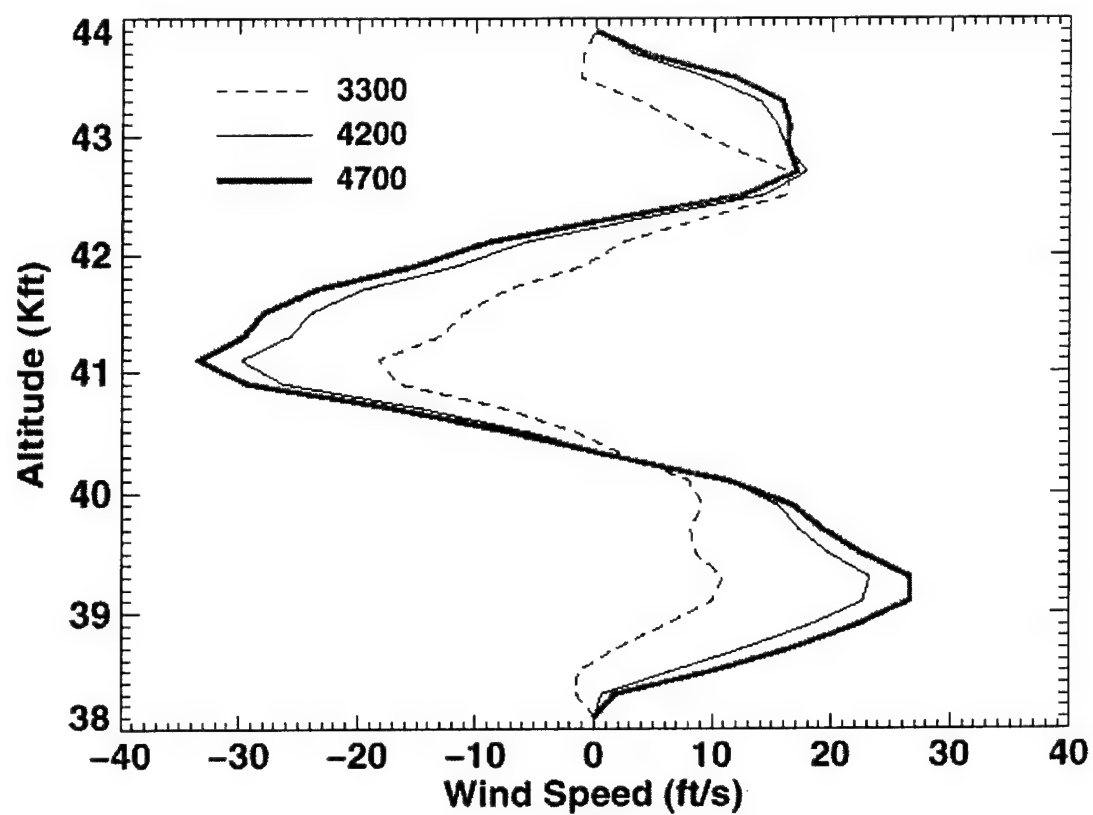


Figure 18. Forcing function comparisons using different λ_a . Taken from Jimsphere profile
WR 10-12-78 03:45Z.

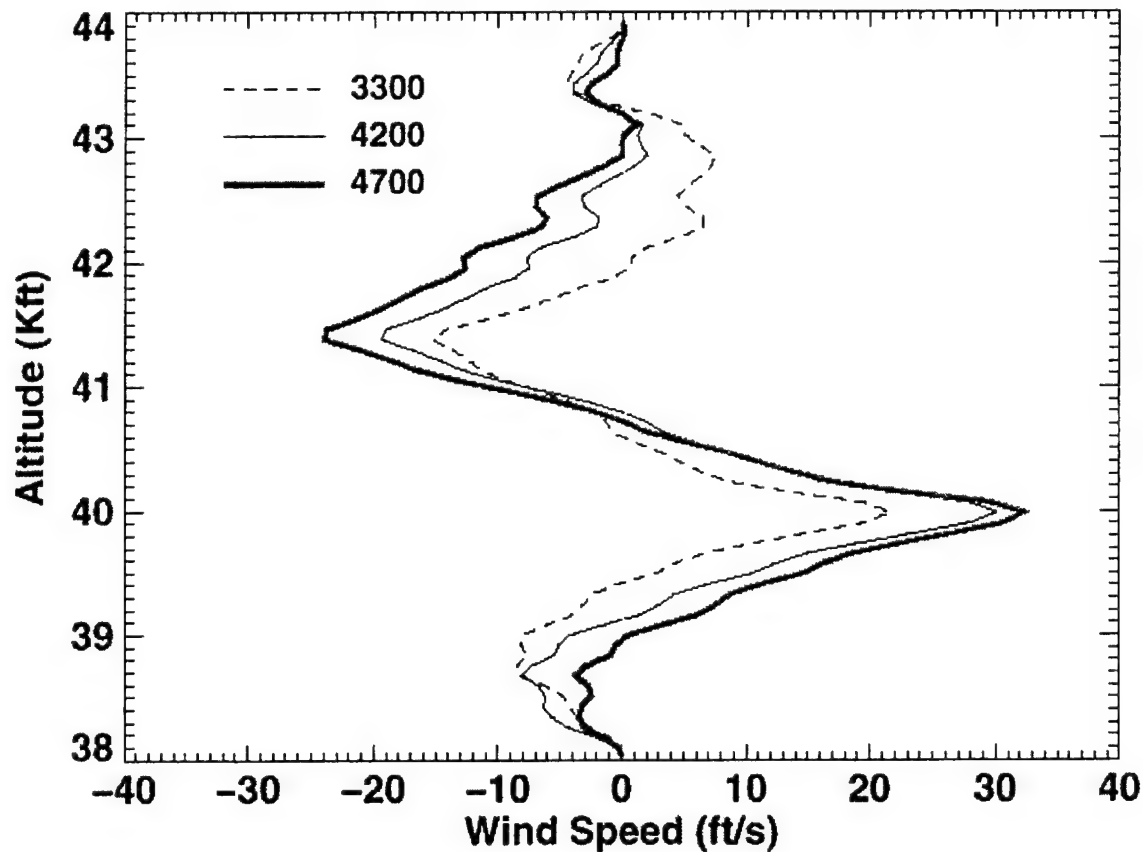


Figure 19. Forcing function comparisons using different λ_0 . Taken from Jimsphere profile WR 05-02-88 19:00Z.

7.1 A Practical Consideration

The primary purpose of this study was to establish the feasibility of deriving from measured wind profiles the turbulent component for use in launch vehicle gust loads analyses. As such, the forcing functions were developed from the total magnitude of the wind. The procedures, as presented herein, are applicable to deriving pairs of north-south and east-west forcing functions that can be applied to a launch vehicle simultaneously.

The forcing functions derived in this paper should not be applied simultaneously to the pitch and yaw planes of a launch vehicle. Moreover, the results of the individual pitch and yaw plane analyses should not be combined without accounting for the fact that each analysis was performed with the total wind turbulence.

8. Conclusions

A methodology for deriving forcing functions from Jimsphere wind profiles that can be used in Monte Carlo gust analyses was presented. Validity of these forcing functions for the wavelengths of interest was established by examining the error contributions from various sources within the wind measurement system and the application of a noise reducing filter. A unique aspect of the method is the extraction of the relatively rapidly changing turbulent component of measured wind profiles.

References

1. Kabe, A. M., "Design and Verification of Launch and Space Vehicle Structures," AIAA-98-1718, April 1998.
2. Smith, S. A., "Revised Gust Model," NASA Marshall Space Flight Center ES44-(147-89), 24 Oct. 1989.
3. Smith, O. E., and Adelfang, S. I., "On the Relationship Between Wind Profiles and the STS Ascent Structural Loads," AIAA paper 89-0709, Jan. 1989.
4. Daniels, G. E., "Natural Environment (Climatic) Criteria Guidelines for Use in MSFC Launch Vehicle Development," 1963 Revision, NASA Marshall Space Flight Center MTP-AERO-63-8, 28 Jan. 1963.
5. Smith, O. E., Adelfang, S. I., and Batts, G., "Wind Models for the NSTS Ascent Trajectory Biasing for Wind Load Alleviation," AIAA-90-0481, Jan. 1990.
6. Haering, E. A., Jr., "Air Data Calibration Techniques for Measuring Atmospheric Wind Profiles," *Journal of Aircraft*, Vol. 29, No. 4, 1992, pp. 632-639.
7. Johnson, D. L., editor, *Terrestrial Environment (Climatic) Criteria Guidelines for Use in Aerospace Vehicle Development*, 1993 Revision, NASA Technical Memorandum 4511, 1993.
8. Johnson, D. L., editor, "National Aerospace Plane (NASP) X-30 Natural Environment Requirements Document (Rev. 1.0)," NASP-NEC-NERD #031594, 15 March 1994.
9. de Jonge, J. B., "Reduction of Incremental Load Factor Acceleration Data to Gust Statistics," Report No. DOT/FAA/CT-94/57, Aug. 1994.
10. Johnson, D. L., NASA Marshall Space Flight Center Document EL23(13-97), "Wind Gust Procedure for Shuttle Ascent," 25 March 1997.
11. Adelfang, S. I., and Smith, O. E., "White Paper - Wind Gust for Shuttle Ascent," 7 March 1997.
12. Adelfang, S. I., and Smith, O. E., "White Paper - Wind Gust for Shuttle Ascent Part II," 14 March 1997.
13. Van Gelder, P. A., "Derivation of Lateral and Vertical Gust Statistics from In-Flight Measurements," AIAA-97-1214, 1997, pp. 673-682.
14. Adelfang, S. I., and Smith, O. E., "Gust Models for Launch Vehicle Ascent," AIAA-98-0747, Jan. 1998.

15. Kim, M. C., Kabe, A. M., Lee, S. S., "Atmospheric Flight Gust Loads Analysis," AIAA-99-1252, April 1999.
16. Fichtl, G. H., "The Response of Rising or Falling Spherical Wind Sensors to Atmospheric Wind Perturbations," *Journal of Applied Meteorology*, Vol. 10, No. 6, Dec. 1971, pp. 1275-1284.
17. DeMandel, R. E., and S. J. Krivo, "Radar/Balloon Measurement of Vertical Air Motions Between the Surface and 15km," *Journal of Applied Meteorology*, Vol. 10, Apr. 1971, pp. 313-319.
18. Wilfong, T., Smith, S., and Crosiar, C., "Characteristics of High-Resolution Wind Profiles Derived from Radar-Tracked Jimspheres and the Rose Processing Program," *Journal of Atmospheric and Oceanic Technology*, Vol 14, Apr. 1997, pp 318-325.
19. Zartarian, G., and Thompson, J. H., "Validity of Detailed Balloon Soundings in Booster Vehicle Design," Air Force Cambridge Research Lab Report, AFCRL-68-0606, Oct. 1968.
20. Luers, J. K., and MacArthur, C. D., "Ultimate Wind Sensing Capabilities of the Jimsphere and Other Rising Balloon Systems, NASA CR-2048, 1972.
21. Eckstrom, C. V., "Theoretical Study and Engineering Development of Jimsphere Wind Sensor, Final Report on Jimsphere Wind Sensor, Final Report on Contract NASA-11158, prepared by the G. T. Schjeldahl Co., for NASA Marshall Space Flight Center, July 1965.
22. Luers, J., and Engler, N., "On Optimum Methods for Obtaining Wind Data from Balloon Sensors," *Journal of Applied Meteorology*, Vol. 6, Oct. 1967, pp. 816-823.
23. Fichtl, G. H., DeMandel, R. E., and Krivo, S. J., "Aerodynamic Properties of Spherical Balloon Wind Sensors," *Journal of Applied Meteorology*, Vol. 11, April 1972, pp. 472-481.
24. Scoggins, J. R., and Susko, M., "FPS-16 Radar/Jimsphere Wind Data Measured at the Eastern Test Range", NASA Technical Memorandum X-53290, July 1965.
25. Engler, N. A., Luers, J. K., and McCloskey, J. W., "An Analysis of the AN/FPS-16 Rose System," Air Force Cambridge Research Lab Report, AFCRL-67-0534, 1967.
26. Engler, N. A., Luers, J. K., McCloskey, J. W., and Strange, J. D., "Tracking Errors in Detailed Wind Soundings," Air Force Cambridge Research Lab Report, AFCRL-69-0213, 1969.
27. VanZandt, T., "A Universal Spectrum of Bouyancy Waves in the Atmosphere," *Geophysical Research Letters*, Vol. 9, May 1982, pp. 575-578.
28. Garrett, C., and Munk, W., "Space-Time Scales of Internal Waves," *Geophysical Fluid Dynamics*, Vol. 2, 1972, pp. 225-264.
29. Garrett, C., and Munk, W., "Space-Time Scales of Internal Waves: A Progress Report," *Journal of Geophysical Research*, Vol. 80, 1975, pp. 291-297.

30. Dewan, E. M., and Good, R. E., "Saturation and the 'Universal' Spectrum for Vertical Profiles of Horizontal Scalar Winds in the Atmosphere," *Journal of Geophysical Research*, 91, D2, 2742-2748, Feb. 1986.
31. Smith, S., Fritts, D., and VanZandt, T., "Evidence for a Saturated Spectrum of Atmospheric Gravity Waves," *Journal of Atmospheric Sciences*, Vol. 44, No. 10, May 1987, pp. 1404-1410.
32. Susko, M., and Vaughan, W. W., "Accuracy of Wind Data Obtained by Tracking Jimsphere Wind Sensor Simultaneously with Two FPS-16 Radars," NASA Technical Memorandum TM X-53752, July 5, 1968.
33. Bendat, J. S., and Piersol, A. G., *Random Data Analysis and Measurement Procedures*, 2nd ed., Wiley-Interscience, N.Y., 1986.
34. Papoulis, A., *Signal Analysis*, McGraw-Hill, 1977, pp. 336-339.
35. Press, W. H., Flannery, B. P., Teukolsky, S. A., and Vetterling, W. T., *Numerical Recipes*, Cambridge Press, 1986, pp. 539-542.
36. Spiekermann, C. E., Sako, B. H., and Kabe, A. M., "Identifying Slowly-Varying and Turbulent Wind Features for Day-of-Launch Flight Loads Analyses," AIAA-99-1250, April 1999.